Cerebral Cortex Advance Access published May 22, 2014

Cerebral Cortex
doi:10.1093/cercor/bhu091

Stimulus Dependence of Gamma Oscillations in Human Visual Cortex

D. Hermes[1,2], K.J. Miller[3,4], B.A. Wandell[2] and J. Winawer[1,5]

[1]Department of Psychology, New York University, New York, NY, USA, [2]Department of Psychology, [3]Department of Neurosurgery, Stanford University, Stanford, CA, USA, [4]Program in Neurobiology and Behavior, University of Washington, Seattle, WA, USA, and [5]Center for Neural Science, New York University, New York, NY, USA

Address correspondence to Dora Hermes, Stanford University, Department of Psychology—Wandell Lab, 450 Serra Mall, Stanford, CA 94305, USA. Email: dhermes@stanford.edu

A striking feature of some field potential recordings in visual cortex is a rhythmic oscillation within the gamma band (30–80 Hz). These oscillations have been proposed to underlie computations in perception, attention, and information transmission. Recent studies of cortical field potentials, including human electrocorticography (ECoG), have emphasized another signal within the gamma band, a nonoscillatory, broadband signal, spanning 80–200 Hz. It remains unclear under what conditions gamma oscillations are elicited in visual cortex, whether they are necessary and ubiquitous in visual encoding, and what relationship they have to nonoscillatory, broadband field potentials. We demonstrate that ECoG responses in human visual cortex (V1/V2/V3) can include robust narrowband gamma oscillations, and that these oscillations are reliably elicited by some spatial contrast patterns (luminance gratings) but not by others (noise patterns and many natural images). The gamma oscillations can be conspicuous and robust, but because they are absent for many stimuli, which observers can see and recognize, the oscillations are not necessary for seeing. In contrast, all visual stimuli induced broadband spectral changes in ECoG responses. Asynchronous neural signals in visual cortex, reflected in the broadband ECoG response, can support transmission of information for perception and recognition in the absence of pronounced gamma oscillations.

Keywords: broadband spectral change, electrocorticography, gamma oscillations, human electrophysiology, visual cortex

Introduction

Recordings of stimulus induced field potentials in visual cortex sometimes show a narrowband increase in spectral power within the gamma range typically peaking ~40–60 Hz (reviewed by Fries et al. 2008). This narrowband response has attracted a great deal of attention because of the suggestion that the oscillations play a key role in perception and cognition (Eckhorn et al. 1988; Gray et al. 1989, 1999; Fries et al. 2007), and because of the related hypothesis that the precise timing of these neural oscillations is critical for information transfer between remote cortical sites (Fries 2005).

Some researchers have made vigorous counterarguments against the functional significance of these oscillations for perception (Shadlen and Movshon 1999; Thiele and Stoner 2003; Roelfsema et al. 2004). Recent studies in nonhuman primates show that the characteristics of narrowband gamma responses depend on the spatial structure of the visual stimulus. For example, the amplitude (Henrie and Shapley 2005) and peak frequency (Ray and Maunsell 2010) of the gamma oscillations increase with grating contrast. Large gamma oscillations can be recorded in response to a large grating stimulus, but the response amplitude is reduced when a perpendicular grating is superimposed to create a plaid pattern (Lima et al. 2010; Bartolo et al. 2011), when noise is superimposed on the grating (Zhou et al. 2008; Jia et al. 2011), when the grating is relatively small (Bauer et al. 1995; Gieselmann and Thiele 2008; Jia et al. 2011; Ray and Maunsell 2011; Jia Xing et al. 2013), or when natural movies are viewed rather than a grating (Kayser et al. 2003). Some researchers have argued that these stimulus-dependent variations in frequency and amplitude of the oscillatory gamma response preclude a role for oscillations in perceptual binding or communication (Ray and Maunsell 2010).

Despite the clear stimulus dependencies of gamma oscillations, hypotheses about a fundamental role of oscillations for vision have not been rejected. Several reasons are offered. First, the fact that parameters of the gamma oscillation depend on stimulus properties might not preclude narrowband gamma oscillations from playing an important role in information transfer (Bosman et al. 2012; Roberts et al. 2013). Second, the absence of gamma oscillations when viewing natural stimuli (Kayser et al. 2003), was explained as a consequence of motion signals in the stimuli masking gamma oscillations rather than the oscillations being sensitive to the spatial structure of the image. Finally, a recent study in nonhuman primates claims that gamma oscillations are elicited in macaque during free viewing of all static natural images (Brunet et al. 2013).

If narrowband gamma oscillations are essential for seeing and recognition (Melloni et al. 2007) and for feedforward information transfer (Bosman et al. 2012), then we expect these oscillations to be elicited by all static, visible stimuli, not just a restricted set—say stimuli with a periodic spatial or temporal structure. Moreover, it is important to analyze the data using methods that distinguish narrowband gamma oscillations, which are indicated by a peak in the spectral response (Lopes da Silva 2013), from broadband signals, which span the gamma range but do not have a distinct peak (Miller, Sorensen et al. 2009). Recent reports have claimed that these 2 signals may originate from different neural circuits (Manning et al. 2009; Ray and Maunsell 2011). Prior reports of gamma oscillations in human intracranial recordings did not always separate these 2 responses (Tallon-Baudry et al. 2005; Crone et al. 2011).

We specifically looked for narrowband gamma oscillations using intracranial recordings in human visual cortex, and we analyzed the dependence of these oscillations on the visual stimulus. We found that static grating stimuli elicited both narrowband gamma and broadband high frequency responses in a large area of visual cortex. The amplitude of the oscillations was large and the narrowband response could be measured on single trials. However, highly visible static noise patterns failed to elicit a narrowband response. Instead, these patterns produced a substantial broadband response. Only a small subset of face and house picture stimuli elicited narrowband oscillations, and these responses were present in only a restricted

region within early visual areas. We could find no gamma oscillations on the fusiform or parahippocampal gyri, regions that appear to be important for perceiving face and house stimuli (Allison et al. 1994; Puce et al. 1995; Parvizi et al. 2012).

The amplitude of the narrowband oscillations depends substantially on the spatial structure of the image, so much so that many plainly visible stimuli do not give rise to narrowband responses. The cortical locations of the oscillations to face and house stimuli are not located in regions thought to be responsible for perception of these objects. We conclude that gamma oscillations do not play an essential role for seeing many types of visual stimuli.

Materials and Methods

Subject and Procedure

ECoG data were measured from 2 subjects who were implanted with subdural electrodes (2.3 mm diameter, AdTech Medical Instrument Corp.) for clinical purposes. All subjects gave informed consent to participate in the study and the study was approved by the Stanford University IRB. During ECoG measurements stimuli were shown on a 15 in. MacBook Pro laptop using Psychtoolbox (http://psychtoolbox.org/). The laptop was placed 60 cm from the subject's eyes at chest level. Screen resolution was 1280 × 800 pixels (33 × 21 cm). In Subject 1, a functional magnetic resonance imaging (fMRI) scan was performed for retinotopic mapping before the implantation of the electrodes and the same experiment was repeated during ECoG (data presented in Winawer et al. 2013, see Supplementary Fig. S1).

Stimuli and Task

In Experiment 1, the subjects viewed static images of gratings and noise patterns for 500 ms each, with 500 ms of zero-contrast (mean luminance) between successive stimuli. Stimuli came from 7 classes (30 exemplars per class, 25 × 25°), including high contrast vertical gratings (0.16, 0.33, 0.65, or 1.3 duty cycles per degree square wave) and noise patterns (spectral power distributions of k/f^4, k/f^2, and k/f^0). Subjects fixated on a dot in the center of the screen that alternated between red and green, changing colors at random times. Subject 1 pressed a button when the fixation dot changed color. Subject 2 fixated the dot but did not make manual responses because these responses were found to interfere with visual fixation.

In Experiment 2, the subject viewed static images of faces or houses (50 each, 10 × 10°) in random order with a small amount of stationary (not moving) white noise superimposed on the image (70% gray-scale image + 30% noise in pixel intensities). Images were presented for durations ranging from 293 to 2625 ms, with a mean ISI of 1838 ms. Only stimuli with durations of at least 460 ms were included in analyses ($n = 99$). The subject indicated whether the image was a face or a house by pressing a button.

ECoG Recording

ECoG data were recorded at 3052/1528 Hz (Subject 1/Subject 2) from 118/96 electrodes through a 128-channel Tucker Davis Technologies recording system (http://www.tdt.com). To localize electrodes, a computed tomography (CT) scan was acquired after electrode implantation and co-registered with a preoperative structural MRI scan. Electrodes were localized from the CT scan and co-registered to the MRI (Hermes et al. 2010). Electrodes that showed large artifacts or showed epileptic activity, as determined by the patient's neurologist (JP) were excluded from analysis (7/35 electrodes were excluded in Subject 1/Subject 2 in Experiment 1 and 13 electrodes were excluded in Experiment 2). Off-line, data were re-referenced to the common average, low pass filtered and resampled at 1000 Hz for computational purposes using the Matlab resample function. Line noise was removed at 60, 120 and 180 Hz using a third order Butterworth filter. Results from the manuscript were unchanged if data were pairwise re-referenced to a "silent" electrode rather than to the common average.

ECoG Analyses

Time Frequency Analysis

To visualize spectral power changes during stimulus presentation, a time frequency analysis was performed around stimulus onset (−200 to 1000 ms) with a multitaper approach (Percival and Walden 1993) using chronux (http://www.chronux.org/ (Mitra and Bokil 2008)). A moving window of 200 ms (with overlap of 50 ms) and the use of 5 tapers result in a frequency resolution of 5 Hz, with a spectral smoothing of ±15 Hz. To normalize the responses to baseline, the average spectrum from all inter trial intervals 250–500 ms after stimulus offset was computed and divided from every time bin. The base 10 log was then computed on this normalized power and plotted (Figs 1 and 4).

Spectral Analysis

To quantify the responses, we calculated power spectra and separated ECoG responses into broadband and narrowband gamma band spectral power increases. To control for the influence of evoked activity on the spectrum, event related potentials (ERPs) were calculated per condition and the condition-specific ERP was regressed from each trial. This procedure makes sure that the broadband increase is not due to a sharp edge in the ERP; the same pattern of results is obtained if this step is omitted. For each condition, the average power spectral density was calculated every 1 Hz by Welch's (1967) method with a 500 ms window (0–500 ms after stimulus onset, and 0–500 ms after stimulus offset for the baseline) and a Hamming window to attenuate edge effects (Fig. 2 and see Supplementary Fig. S2). ECoG data are known to obey a power law and to capture broadband and narrowband gamma increases separately the following function (F) was fitted to the average log spectrum from 35 to 200 Hz (leaving out 60 Hz line noise and harmonics) from each condition:

$$P(x) = (\beta_{\text{broadband}} - n\mathrm{x}) + \beta_{\text{narrowband}} G(\mathrm{x}|\mu, \sigma) \qquad (1)$$

In which,

$$x = \log10(\text{frequency})$$
$$G(\mathrm{x}|\mu, \sigma) = e^{-(x-\mu)^2/2\sigma^2}$$

with $10^{\sigma} = 1.1$ Hz and 35 Hz $< 10^{\mu} <$ 80 Hz.

The slope of the log–log spectral power function (n) was fixed for each electrode by fitting it based on the average power spectrum of the baseline. To estimate whether broadband and gamma increases were significant, confidence intervals were calculated by a bootstrap procedure. For each condition C with N_c trials, N_c trials were drawn randomly with replacement and power spectra were averaged. The function P is the average log-power spectrum from these trials and the parameters β were fitted. This was repeated 100 times, resulting in a distribution of broadband and narrowband weights. Effects are reported as significant if the 95% overlapping confidence intervals were not overlapping with the 95% confidence interval from the baseline period, and are not further corrected for multiple comparisons across electrodes.

Example Datasets and Software Code

In the interest of reproducible scientific computation (Gavish and Donoho 2012; LeVeque et al. 2012), the full Matlab code and sample data used to create Figures 1, 2, 3, 4B and 5 are made available in the Supplementary Materials.

Results

In one experiment, we measured responses to square wave gratings of different spatial frequencies and noise patterns with several amplitude spectra. In a second experiment, we

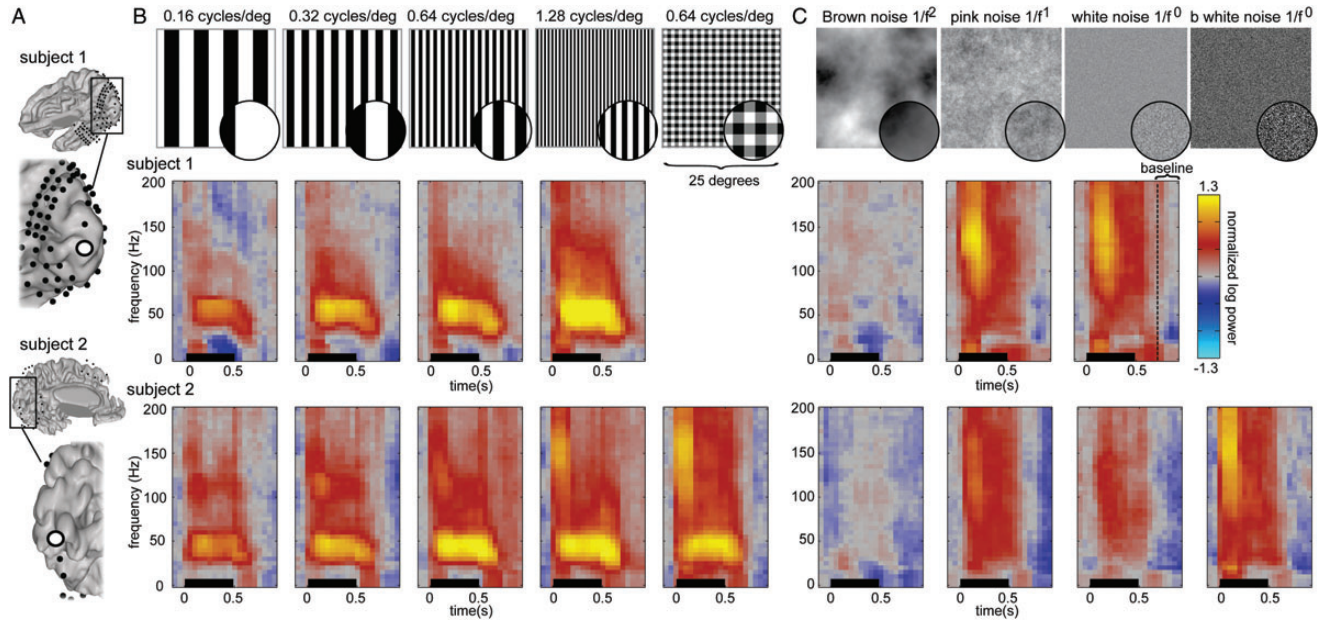

Figure 1. Time–frequency power estimates in V1/V2 for gratings and noise stimuli. (*A*) ECoG electrode locations in Subjects 1 and 2. (*B*) Grating stimuli were presented for 500 ms, insets in circles show a magnified portion of the stimuli for visibility. Time–frequency power estimates ("spectrograms") from an electrode in V1/V2 from Subject 1 (top row) and Subject 2 (bottom row). (*C*) Noise patterns were presented for 500 ms. Spectrograms from the same early visual electrode in Subject 1 (top row) and Subject 2 (bottom row). All spectrograms are normalized with respect to the same baseline: the inter-stimulus interval between all trials (from 750–1000 ms after stimulus onset). Spectrograms are cut off at a maximum of ± 1.3 $\log_{10}$ units. The multitaper approach results in a temporal smoothing of 200 ms and a frequency smoothing of ± 15 Hz. Spectrograms represent averages across all trials of a given type.

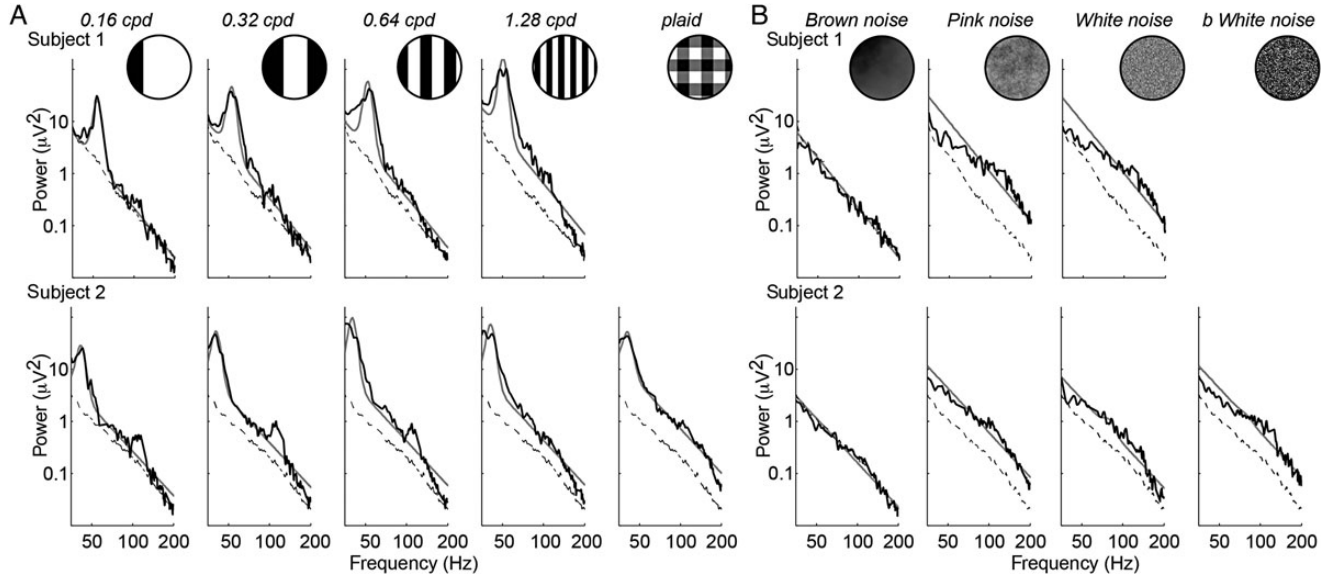

Figure 2. Power spectra in V1/V2 for gratings and noise stimuli. Power spectra to the grating stimuli for the same electrodes shown in Figure 1 on a log–log plot (top, Subject 1; bottom, Subject 2). The black line shows the power spectrum from the grating stimuli (*A*) and noise stimuli (*B*). The dashed line shows the power spectrum from the baseline periods. A line plus Gaussian (model) was fitted to the average power spectra of each condition (data) in log–log space, resulting in one weight for broadband and one weight for narrowband increases relative to baseline. The fit from this model is plotted in gray.

measured responses to images of faces and houses. For all stimuli in both experiments, the spectral responses were modeled as the sum of 3 components: a baseline, a narrowband gamma signal, and a broadband signal (Winawer et al. 2013). Quantitatively modeling the responses enables us to test for stimulus specificity of both types of signals across several areas in visual cortex.

Gratings, but Not Noise Patterns, Elicit Narrowband Gamma

Measurements were made in visual cortex in 2 subjects. To illustrate the principles, we first consider responses in 2 electrodes (one from each subject) located near the foveal representation at the V1/V2v border (Fig. 1A). We then discuss a more extensive set of data.

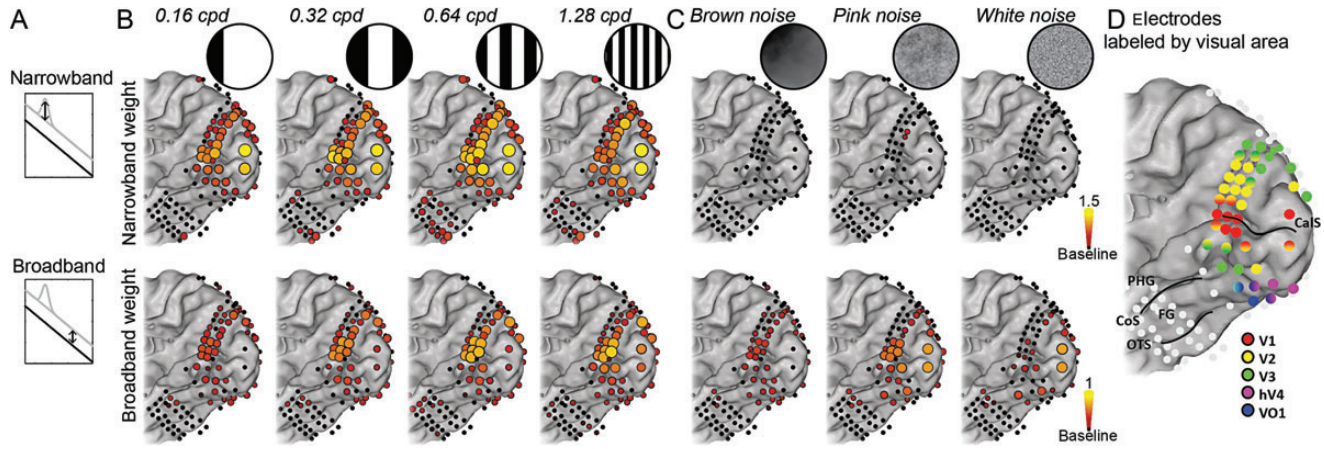

Figure 3. Spatial distribution of narrowband (gamma) and broadband weights. (*A*) Spectral power changes during visual stimulation compared with baseline were separated in increases in narrowband gamma rhythms and broadband increases by fitting a power law shape with a Gaussian. (*B*) Spatial distribution of narrowband gamma (top) and broadband weights (bottom) in Subject 1 during grating stimuli. (*C*) Spatial distribution of narrowband gamma (top) and broadband weights (bottom) in Subject 1 during noise stimuli. Electrodes that showed a significant increase compared with baseline are plotted in color on the rendered brain surface ($P < 0.05$ uncorrected). (*D*) ECoG electrodes labeled by visual field mapping experiment (Winawer et al. 2013). CalS = calcarine sulcus, PHG = parahippocampal gyrus, CoS = collateral sulcus, FG = fusiform gyrus, and OTS = occipital-temporal sulcus.

The ECoG responses differ strikingly as a function of the spatial pattern in the stimuli. Here, we show the complete response spectrograms from both subjects to square wave gratings at several spatial frequencies (Fig. 1B) and several types of noise patterns (Fig. 1C). The power spectra are shown in Figure 2. In all cases, the square wave stimuli elicited robust narrowband gamma responses, peaking near 50 Hz (Figs 1B and 2A). This response duration is sustained for the entire stimulus duration (0.5 s). These ECoG oscillations are consistent with local field potential (LFP) recordings in animal and magnetoencephalography (MEG) and electroencephalography (EEG) recordings in human (Fries et al. 2008).

There is also a spectrally broadband response elevation. The broadband response spans a wide range of frequencies, from 50–200 Hz (upper limit due to the noise floor). This response begins slightly earlier in time (50–100 ms) than the narrowband response. It is larger at stimulus onset and then continues at a lower level for the stimulus duration. The amplitude of the broadband response increases as the fundamental spatial frequency of the grating stimuli rises from 0.16 to 1.28 cycles per degree.

The responses to the spatial noise patterns are very different from the responses to the gratings (Figs 1C and 2B). The noise stimuli produce a broadband elevation in spectral power, but there are no narrowband gamma oscillations. The broadband response to the noise stimuli is similar to the broadband response to the gratings; the amplitude is largest at stimulus onset and then continues throughout the stimulus presentation but at a lower level (Fig. 2C).

The response pattern in the foveal V1/V2 electrodes in the 2 subjects shown in Figures 1 and 2 is replicable across >30 other cortical locations (Fig. 3). Across visual sites, the response is well approximated as a mixture of a narrowband gamma oscillation and a broadband response. To summarize the measurements, we modeled the power spectrum as the weighted sum of 2 components in log-power by log-frequency plot: (1) a straight line from 35 to 200 Hz (broadband) and (2) a Gaussian centered between 35 and 80 Hz (gamma band oscillation) (Equation 1; see Supplementary Fig. S2). This allowed us to visualize the spatial distribution of the 2 signal components across the electrode arrays.

Nearly all electrodes (33/34) in visual areas V1/V2/V3 show a significant narrowband gamma response to at least one of the square wave gratings (Fig. 3B, top). Most (31/34) also have a significant broadband response (Fig. 3B, bottom see Supplementary Fig. S2). For the noise patterns, however, only 2 electrodes on V1/V2/V3 have measurable gamma responses (Fig. 3C, top, pink noise condition). These 2 electrodes were not located near the foveal representation.

Most V1/V2/V3 electrodes (28/34) have a significant broadband response to at least one of the 3 types of noise stimuli (Fig. 3C, bottom; see Supplementary Fig. S2). Broadband responses in the fovea are larger for white and pink noise than for Brown noise patterns, consistent with the observation that foveal V1/V2/V3 is less sensitive to low spatial frequencies (Wandell 1995), which dominate the Brown noise stimuli. Peripheral electrodes show the opposite pattern: a larger broadband response to the Brown noise stimuli than the white noise stimuli. This spatial pattern is consistent with the fact that the periphery is more sensitive to low spatial frequencies. The ventral occipital-temporal electrodes responded occasionally, but weakly, to both grating and noise stimuli.

The Spatial Distribution of Broadband and Narrowband Responses to Object Stimuli Differ

Next, we measured responses to face and house picture stimuli (Subject 1; Fig. 4). During the ECoG recording, the subject correctly indicated for each image whether it was a face or a house ($n = 99$, mean reaction time ± standard deviation (SD): 682 ± 160 ms for faces and 726 ± 202 ms for houses). There was little narrowband gamma evoked in electrodes near the foveal representation in V1/V2. Spectrograms from the V1/V2 electrode with the strongest narrowband gamma response are shown in Figure 4B. In foveal V1/V2, 0 of 2 electrodes showed significant narrowband gamma responses for faces, 1 of 2 for houses (Fig. 4C). Narrowband gamma responses were not observed in the fusiform nor parahippocampal gyri. Some weak but significant gamma oscillations were observed in peripheral V1/V2/V3, in cortical regions that represent the visual field position at the stimulus edge.

The spatial pattern of broadband responses is quite different from the pattern of narrowband responses (Fig. 4C). The

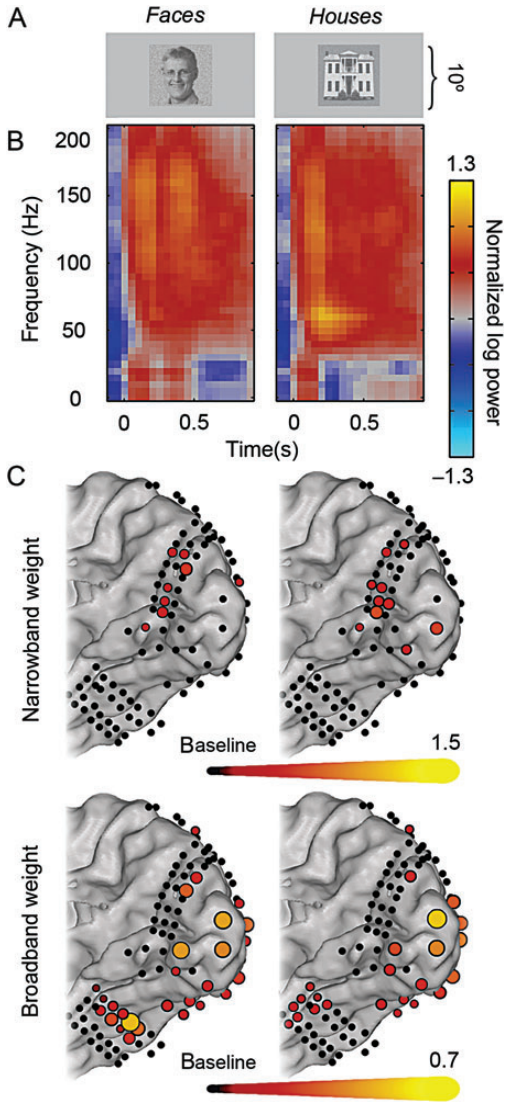

Figure 4. Spectral power changes during face and house viewing. (*A*) Examples of face and house stimuli presented during experiment 2. (*B*) Spectrograms from an early visual electrode in Subject 1 (Fig. 1*A*) while seeing faces (left) and houses (right). (*C*) Spatial distribution of significant increases in narrowband and broadband weights ($P < 0.05$ uncorrected). Early visual areas show little or no narrowband gamma increases while viewing faces (top left) and houses (top right), but large increases in broadband power (bottom). The fusiform gyrus and parahippocampal gyrus show significant broadband increases, but no gamma increases, while viewing faces and houses, respectively.

distribution of this activity is similar to the pattern observed in functional MRI experiments. The largest response is near the occipital pole (in the 2 electrodes on foveal V1/V2). This is expected because these stimuli subtended a relatively small visual angle (10° diameter). In addition, significant broadband responses were measured on the fusiform gyrus for face stimuli and on the parahippocampal gyrus for house stimuli, consistent with the location of face- and place-selective regions of ventral temporal cortex (Allison et al. 1994; Puce et al. 1995; Kanwisher et al. 1997; Aguirre et al. 1998; Epstein and Kanwisher 1998).

Individual Trial Analysis

Noise patterns did not elicit reliable gamma oscillations on single trials; but gratings did. For an electrode on the boundary of foveal V1/V2, the narrowband gamma responses to the noise stimuli were beyond the 50% confidence interval defined by the baseline period response for only 4 of 90 trials (Fig. 5A, top). For the highest spatial frequency grating stimuli, the narrowband gamma responses were beyond the 50% confidence interval of the baseline periods on 28 of 30 trials (Fig. 5A, top).

A broadband response was measured on nearly every trial with stimuli containing relatively high spatial frequency patterns (pink and white noise patterns; gratings of 1.3 cpd) (Fig. 5A, bottom). The relative insensitivity of a foveal V1/V2 electrode to very low spatial frequencies (0.16 cpd grating and brown noise patterns) is expected (Wandell 1995).

For face and house stimuli, the narrowband gamma responses were mostly in the baseline range (Fig. 5B, top). For a few trials, however, narrowband gamma responses exceeded baseline. The broadband responses to faces and houses were reliably outside the baseline range (Fig. 5B, bottom).

Discussion

Narrowband gamma responses to certain stimuli can be reliably measured with ECoG in human visual cortex. In this general sense, there is agreement between ECoG and MEG/EEG in human, and LFP measurements in cat and macaque (reviewed by Fries et al. 2008). When present, the ECoG narrowband oscillations are substantially (~1.5 $\log_{10}$ units) above baseline and they can be observed on individual trials.

However, many types of static, visible stimuli fail to elicit narrowband gamma oscillations. Three different types of noise patterns fail to elicit narrowband gamma oscillations. Many pictures of faces and houses tested do not elicit gamma oscillations.

The broadband response amplitude and position is in much better agreement with excitations expected from visible stimuli. With the exception of spatial frequency inappropriate stimuli (low frequencies in the fovea and high frequencies in the periphery), all the stimuli used in this study produce a general (broadband) response that spanned all frequencies from ~80 Hz up to the noise floor. The broadband responses to face and house stimuli were clearly present in ventral occipital regions that are thought to be important for recognizing these images.

Gamma Oscillations are Stimulus Specific

The failure to observe narrowband gamma responses to certain classes of stimuli cannot be explained by the experimental setting or signal contamination. In electrodes where grating stimuli generate clear narrowband gamma as well as broadband responses, other types of stimuli in the same visual field positions produce robust single trial broadband responses in the absence of gamma oscillations. It is unlikely that the stimuli that did not elicit gamma rhythms were not perceived, because all stimuli were large (at least 10 × 10°), had an abrupt onset during central fixation, and remained on the screen for at least 500 ms, sufficiently long to allow for conscious perception (Dehaene and Changeux 2011). Moreover, the grating stimuli (which reliably elicited gamma oscillations) and the noise stimuli (which did not) were randomly interleaved and presented at a rapid rate (1 stimulus per second), ruling out the possibility that the subjects' attentional state differed between the stimulus classes. Finally, the behavioral performance during the face and house experiment

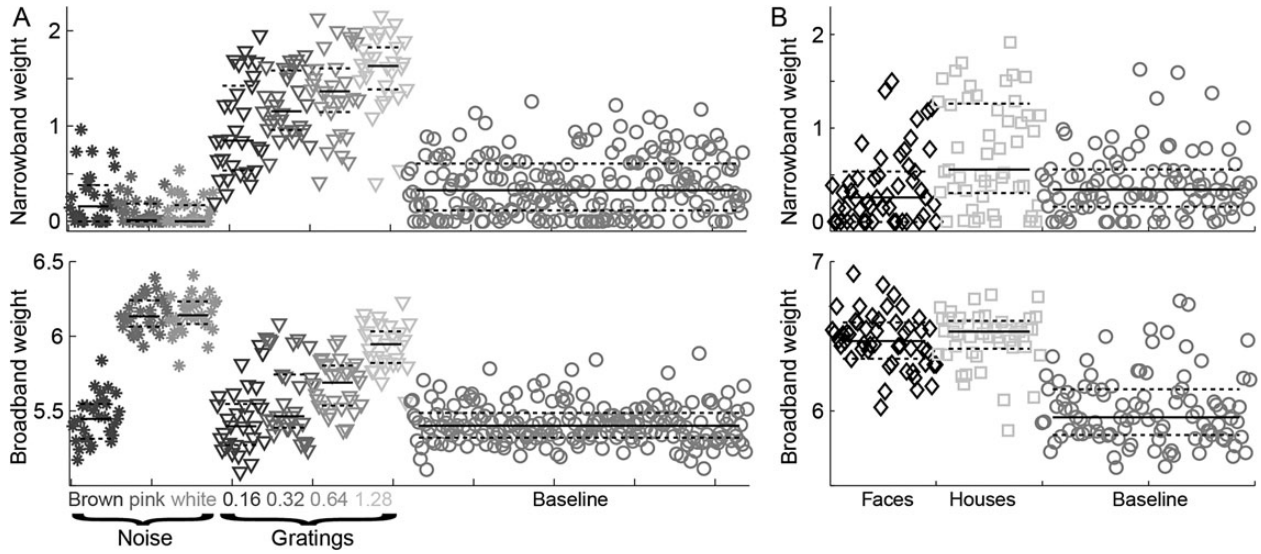

Figure 5. Narrowband (gamma) and broadband power in individual trials. (*A*) Increases in narrowband gamma (top row) and broadband (bottom row) in a V1/V2 electrode in Subject 1 during all individual trials of Experiment 1. Horizontal bars indicate the median (solid) and quartiles (dotted) for each condition. (*B*) The same for Experiment 2. This electrode shows increased gamma oscillations for only some face and house stimuli, it shows a broadband increase for almost all stimuli.

showed that the subject correctly labeled all stimuli ($n = 99$ trials) as a face or a house.

A previous report showed that in macaque LFP recordings, narrowband gamma oscillations are observed in response to high contrast gratings but not low contrast gratings (Henrie and Shapley 2005). In our experiments, the noise stimuli and the gratings had the same luminance range, and the binary white noise stimuli and the gratings had the same luminance variance. Hence the absence of gamma oscillations in response to the noise patterns is not a result of low spatial contrast. Some spatial patterns do not elicit gamma oscillations.

The lack of narrowband oscillations to the noise patterns cannot be due to a lack of coherent spatial structure or recognizable content in the images. Images containing faces and houses with moderate white noise superimposed did not lead to consistent gamma band oscillations in the expected locations in visual cortex, despite the fact that the subject attended to and accurately classified the images as faces or houses.

Exactly which stimulus features are necessary to elicit gamma oscillations is unclear. As we show, noise patterns do not have the necessary features. It appears that gratings and bars reliably elicit gamma oscillations in humans (Figs 1–3, 5 and Hoogenboom et al. 2006) as well as animals (Gray and Singer 1989; Gray et al. 1989). Important features of the oscillation such as its peak frequency and amplitude depend on specific stimulus features such as color (Swettenham et al. 2013), contrast (Henrie and Shapley 2005; Ray and Maunsell 2010), spatial area (Bauer et al. 1995; Gieselmann and Thiele 2008; Jia et al. 2011; Ray and Maunsell 2011; Jia Xing et al. 2013), noise masking (Zhou et al. 2008; Jia and Kohn 2011; Jia Tanabe et al. 2013), and the number of orientations (Lima et al. 2010; Bartolo et al. 2011).

A recent ECoG measurement in macaque showed that gamma oscillations were elicited during the free viewing of natural images (Brunet et al. 2013). The gamma response was present for several of the images shown and in the mean response across all images. In a re-analysis of a dataset used for another study (Parvizi et al. 2012; Jacques et al. 2013), we quantified the narrowband gamma response to 72 images of faces, houses, limbs, and cars (see Supplementary Fig. S3). It is likely that our results are consistent with those of Brunet et al. (2013) in one sense: some natural images elicit narrowband gamma oscillations in visual cortex. Consequently, the mean across all stimuli is above zero.

However, many images do not elicit significant gamma oscillations in V1 (32 and 33 of 72 images for 2 V1 electrodes). The lack of gamma oscillations observed for nearly half the stimuli is unlikely to be due to measurement artifacts, as nearly all stimuli elicited a significant broadband response (69 and 68 of 72 images for the same 2 electrodes). Figure 6 shows 2 example images, one that produces a large gamma oscillation and one that does not. These images were viewed 6 times each and the amplitude of the broadband and narrowband responses was reliable across the repetitions, but different between stimuli. All of the images contained recognizable objects or scenes; the fact that many failed to elicit clear gamma oscillations indicates that this response depends on the spatial structure of the image, and is not likely to be necessary for perception, attention, or recognition. We cannot rule out the possibility that for stimuli near detection or recognition threshold, the presence or absence of gamma oscillations will modulate an observer's judgments. However, since very large differences in the gamma response can be observed across different stimuli, it is unlikely that the gamma amplitude is the principal determinant of stimulus detection or recognition.

We conclude that narrowband gamma oscillations are stimulus specific. Principles of information transfer that are governed by gamma oscillations, such as increased coherence between sites for attended stimuli (Womelsdorf et al. 2007), may hold for specific stimulus patterns that produce gamma oscillations, but are not likely to hold generally across different types of stimuli (for an example, see Supplementary Fig. S4).

Predicting which stimuli will elicit a narrowband gamma response and predicting the parameters of that response will require a more complete model. There has been some progress modeling the local neural circuits that give rise to gamma oscillations in neocortex. For example, *in vitro* measurements show

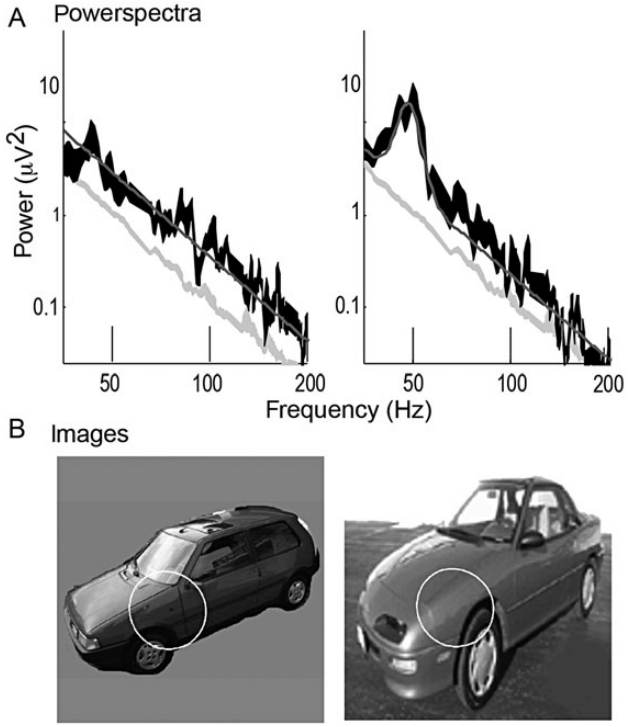

Figure 6. Two example stimuli that induced different levels of narrowband gamma power in V1. (*A*) Power spectra from a foveal V1 electrode for 2 example stimuli (from a set of 72 stimuli, see Supplementary Fig. S3) that were shown to a separate subject in a prior study (Parvizi et al. 2012). Each stimulus was shown 6 times in random order. The 95% confidence intervals are shown in black and the baseline periods are shown in light gray. The baseline is identical for all images. The model fits (power law plus Gaussian) are plotted as a dark gray line. (*B*) The 2 images with the population receptive field (pRF) from the measured electrode indicated by a white circle (2 SD of the pRF Gaussian). The pRF models were obtained from a prior study (Winawer et al. 2013). The car image on the left elicited only a broadband response but no clear gamma oscillation. The car image on the right elicited both a broadband response and a large gamma oscillation.

that gamma oscillations can be driven by the interactions between principal cells and interneurons (Llinas et al. 1991; Whittington et al. 1995; Cunningham et al. 2004), and computational models have been developed to capture these interactions (Wang 2010). One possibility is that regularized spatial patterns projected to visual cortex might be traded for a regularized "reverberation" timescale in recurrent feedback between principal cell and interneuron synaptic connections, reflected by the frequency of gamma oscillations (20–25 ms for feedback corresponding to a 40–50 Hz oscillation). More work is needed to define the stimulus-driven inputs that set up the conditions to produce these oscillations.

Broadband Spectral Power Elevation is Observed for All Visual Stimuli Tested

The stimulus features that give rise to the broadband ECoG signals in visual cortex, unlike the features which give rise to gamma oscillations, are qualitatively well-matched to expectations from other functional measurements, such as fMRI and single unit measurements in animals. All stimuli with spatial contrast patterns induced robust broadband signals across V1/V2/V3, with the exception of stimuli confined to very low spatial frequencies that only elicited broadband signals in more peripheral electrodes, and stimuli dominated by high frequencies, which only elicited broadband signals in more foveal electrodes. Furthermore, broadband ECoG responses to faces and houses arise in the same regions known to be activated in fMRI measurements (Puce et al. 1995; Kanwisher et al. 1997; Aguirre et al. 1998; Epstein and Kanwisher 1998).

Although human MEG and EEG recordings sometimes show narrowband oscillations (Hoogenboom et al. 2006; Vidal et al. 2006; Muthukumaraswamy et al. 2009; Scheeringa et al. 2011; van Pelt and Fries 2013), human ECoG measurements typically show an increase in broadband amplitude (for a review see Crone et al. 2011 and for recordings in early visual cortex see Harvey et al. 2013; Winawer et al. 2013). Although these broadband responses often extend into the gamma range, they should not be considered oscillations, as the spectra are not peaked (Ray and Maunsell 2011; Lopes da Silva 2013). A previous human ECoG study reported gamma oscillations in visual cortex (Tallon-Baudry et al. 2005), but from analyses and figures these narrowband responses are often not separable from broadband responses. Because broadband increases can span frequencies in which oscillations are typically observed (30–80 Hz) (Miller, Sorensen et al. 2009; Harvey et al. 2013; Winawer et al. 2013), decomposing the signal into 2 frequency bins (e.g., 50–80 and 100–200 Hz) may not adequately separate the 2 responses. We fit a model to the spectrum to differentiate between these 2 phenomena; other methods have also been developed to separate narrowband and broadband changes in the ECoG power spectrum (Miller, Zanos et al. 2009; Winawer et al. 2013).

Implications for Theories of Brain Function

Only certain stimuli, such as gratings, reliably produce neural responses that drive resonant (narrowband) gamma oscillations in visual cortex circuits. However, all the stimuli used in this study produce a general (broadband) response. Gamma oscillations and broadband responses do not just differ in the frequency range in which they occur; they also differ in that one has a narrow peak and one does not, reflecting different underlying circuit properties (Manning et al. 2009; Miller, Sorensen et al. 2009; Ray and Maunsell 2011). Understanding the relationship between the stimulus and the 2 responses is likely to clarify fundamental aspects of the circuitry in visual cortex.

For certain stimuli, the power in gamma oscillations is poorly matched to the amplitude of multi-unit activity, in that stimulus manipulations may increase one signal and decrease the other (Bartolo et al. 2011; Ray and Maunsell 2011). Spectrally broadband signals, in contrast, are likely better matched to the total neural activity in nearby regions, reflecting the rate of either input (Miller, Sorensen et al. 2009) or output (Ray and Maunsell 2011) action potentials. Hence when a large spectral peak is observed in a field potential recording, it does not imply that there is a large underlying neural response; it may be a relatively small response that is highly synchronized. In contrast, a large broadband response is more likely to indicate a large neural response. It is likely that perceptual phenomena and other physiological measures such as the BOLD signal will depend in different ways on these circuits.

Broadband and narrowband gamma signals thus indicate different neurophysiological processes. Gamma oscillations may serve a function of information transfer, but only for certain types of visual stimuli that produce a gamma oscillation. Theories about the role of gamma oscillations in visual

information processing that do not incorporate stimulus properties are at best incomplete.

Supplementary Material

Supplementary material can be found at: http://www.cercor.oxfordjournals.org/

Funding

This work was supported by National Eye Institute at National Institutes of Health grant RO1-EY03164 (B.A.W.), National Eye Institute at National Institutes of Health grant R00-EY022116 (J. W.), the Dean's Postdoctoral Fellowships program from the Stanford University School of Medicine (D.H.), National Institutes of Health grant RO1-EY02231801A1 (Kalanit Grill Spector) and Belgian Fund for Scientific Research (FNRS) and Belgian Federal Science Policy Office (BELSPO) (Corentin Jacques).

Notes

The authors thank Josef Parvizi for experimental environment, patient recruitment, and collaborative spirit; Vinitha Rangarajan for her help in data collection; Brett Foster for his help in data collection and helpful discussions; Kendrick Kay for helpful discussions; and Corentin Jacques, Kalanit Grill-Spector, and Nathan Witthoft for providing the data for Figure 6 and Supplementary Figure S3.

References

Aguirre GK, Zarahn E, D'Esposito M. 1998. An area within human ventral cortex sensitive to "building" stimuli: evidence and implications. Neuron. 21:373–383.

Allison T, Ginter H, McCarthy G, Nobre AC, Puce A, Luby M, Spencer DD. 1994. Face recognition in human extrastriate cortex. J Neurophysiol. 71:821–825.

Bartolo MJ, Gieselmann MA, Vuksanovic V, Hunter D, Sun L, Chen X, Delicato LS, Thiele A. 2011. Stimulus-induced dissociation of neuronal firing rates and local field potential gamma power and its relationship to the resonance blood oxygen level-dependent signal in macaque primary visual cortex. Eur J Neurosci. 34:1857–1870.

Bauer R, Brosch M, Eckhorn R. 1995. Different rules of spatial summation from beyond the receptive field for spike rates and oscillation amplitudes in cat visual cortex. Brain Res. 669:291–297.

Bosman CA, Schoffelen JM, Brunet N, Oostenveld R, Bastos AM, Womelsdorf T, Rubehn B, Stieglitz T, De Weerd P, Fries P. 2012. Attentional stimulus selection through selective synchronization between monkey visual areas. Neuron. 75:875–888.

Brunet N, Bosman CA, Roberts M, Oostenveld R, Womelsdorf T, De Weerd P, Fries P. 2013. Visual Cortical gamma-band activity during free viewing of natural images. Cereb Cortex. doi: 10.1093/cercor/bht280.

Crone NE, Korzeniewska A, Franaszczuk PJ. 2011. Cortical gamma responses: searching high and low. Int J Psychophysiol. 79:9–15.

Cunningham MO, Whittington MA, Bibbig A, Roopun A, LeBeau FE, Vogt A, Monyer H, Buhl EH, Traub RD. 2004. A role for fast rhythmic bursting neurons in cortical gamma oscillations in vitro. Proc Natl Acad Sci U S A. 101:7152–7157.

Dehaene S, Changeux JP. 2011. Experimental and theoretical approaches to conscious processing. Neuron. 70:200–227.

Eckhorn R, Bauer R, Jordan W, Brosch M, Kruse W, Munk M, Reitboeck HJ. 1988. Coherent oscillations: a mechanism of feature linking in the visual cortex? Multiple electrode and correlation analyses in the cat. Biol Cybern. 60:121–130.

Epstein R, Kanwisher N. 1998. A cortical representation of the local visual environment. Nature. 392:598–601.

Fries P. 2005. A mechanism for cognitive dynamics: neuronal communication through neuronal coherence. Trends Cogn Sci. 9:474–480.

Fries P, Nikolic D, Singer W. 2007. The gamma cycle. Trends Neurosci. 30:309–316.

Fries P, Scheeringa R, Oostenveld R. 2008. Finding gamma. Neuron. 58:303–305.

Gavish M, Donoho DL. 2012. Three dream applications of verifiable computational results. Comput Sci Eng. 14:26–31.

Gieselmann MA, Thiele A. 2008. Comparison of spatial integration and surround suppression characteristics in spiking activity and the local field potential in macaque V1. Eur J Neurosci. 28:447–459.

Gray CM. 1999. The temporal correlation hypothesis of visual feature integration: still alive and well. Neuron. 24:31–47. 111–125.

Gray CM, Konig P, Engel AK, Singer W. 1989. Oscillatory responses in cat visual cortex exhibit inter-columnar synchronization which reflects global stimulus properties. Nature. 338:334–337.

Gray CM, Singer W. 1989. Stimulus-specific neuronal oscillations in orientation columns of cat visual cortex. Proc Natl Acad Sci U S A. 86:1698–1702.

Harvey BM, Vansteensel MJ, Ferrier CH, Petridou N, Zuiderbaan W, Aarnoutse EJ, Bleichner MG, Dijkerman HC, van Zandvoort MJ, Leijten FS et al. 2013. Frequency specific spatial interactions in human electrocorticography: V1 alpha oscillations reflect surround suppression. Neuroimage. 65:424–432.

Henrie JA, Shapley R. 2005. LFP power spectra in V1 cortex: the graded effect of stimulus contrast. J Neurophysiol. 94:479–490.

Hermes D, Miller KJ, Noordmans HJ, Vansteensel MJ, Ramsey NF. 2010. Automated electrocorticographic electrode localization on individually rendered brain surfaces. J Neurosci Methods. 185:293–298.

Hoogenboom N, Schoffelen JM, Oostenveld R, Parkes LM, Fries P. 2006. Localizing human visual gamma-band activity in frequency, time and space. Neuroimage. 29:764–773.

Jacques C, Witthoft N, Weiner KS, Foster BL, Miller KJ, Hermes D, Parvizi J, Grill-Spector K. 2013. Electrocorticography of category-selectivity in human ventral temporal cortex: spatial organization, responses to single images, and coupling with fMR. J Vis. 13:495.

Jia X, Kohn A. 2011. Gamma rhythms in the brain. PLoS Biol. 9: e1001045.

Jia X, Smith MA, Kohn A. 2011. Stimulus selectivity and spatial coherence of gamma components of the local field potential. J Neurosci. 31:9390–9403.

Jia X, Tanabe S, Kohn A. 2013. Gamma and the coordination of spiking activity in early visual cortex. Neuron. 77:762–774.

Jia X, Xing D, Kohn A. 2013. No consistent relationship between gamma power and peak frequency in macaque primary visual cortex. J Neurosci. 33:17–25.

Kanwisher N, McDermott J, Chun MM. 1997. The fusiform face area: a module in human extrastriate cortex specialized for face perception. J Neurosci. 17:4302–4311.

Kayser C, Salazar RF, Konig P. 2003. Responses to natural scenes in cat V1. J Neurophysiol. 90:1910–1920.

LeVeque RJ, Mitchell IM, Stodden V. 2012. Reproducible Research for Scientific Computing: Tools and Strategies for Changing the Culture. Comput Sci Eng. 14:13–17.

Lima B, Singer W, Chen NH, Neuenschwander S. 2010. Synchronization dynamics in response to plaid stimuli in monkey V1. Cereb Cortex. 20:1556–1573.

Llinas RR, Grace AA, Yarom Y. 1991. In vitro neurons in mammalian cortical layer 4 exhibit intrinsic oscillatory activity in the 10- to 50-Hz frequency range. Proc Natl Acad Sci U S A. 88:897–901.

Lopes da Silva F. 2013. EEG and MEG: Relevance to Neuroscience. Neuron. 80:1112–1128.

Manning JR, Jacobs J, Fried I, Kahana MJ. 2009. Broadband shifts in local field potential power spectra are correlated with single-neuron spiking in humans. J Neurosci. 29:13613–13620.

Melloni L, Molina C, Pena M, Torres D, Singer W, Rodriguez E. 2007. Synchronization of neural activity across cortical areas correlates with conscious perception. J Neurosci. 27:2858–2865.

Miller KJ, Sorensen LB, Ojemann JG, den Nijs M. 2009. Power-law scaling in the brain surface electric potential. PLoS Comput Biol. 5: e1000609.

Miller KJ, Zanos S, Fetz EE, den Nijs M, Ojemann JG. 2009. Decoupling the cortical power spectrum reveals real-time representation of individual finger movements in humans. J Neurosci. 29:3132–3137.
Mitra P, Bokil H. 2008. Observed brain dynamics. New York: Oxford University Press.
Muthukumaraswamy SD, Edden RA, Jones DK, Swettenham JB, Singh KD. 2009. Resting GABA concentration predicts peak gamma frequency and fMRI amplitude in response to visual stimulation in humans. Proc Natl Acad Sci U S A. 106:8356–8361.
Parvizi J, Jacques C, Foster BL, Witthoft N, Rangarajan V, Weiner KS, Grill-Spector K. 2012. Electrical stimulation of human fusiform face-selective regions distorts face perception. J Neurosci. 32: 14915–14920.
Percival DB, Walden A. 1993. Spectral analysis for physical applications, multitaper and conventional univariate techniques. Cambrigde, UK: Cambridge UP.
Puce A, Allison T, Gore JC, McCarthy G. 1995. Face-sensitive regions in human extrastriate cortex studied by functional MRI. J Neurophysiol. 74:1192–1199.
Ray S, Maunsell JH. 2010. Differences in gamma frequencies across visual cortex restrict their possible use in computation. Neuron. 67:885–896.
Ray S, Maunsell JH. 2011. Different origins of gamma rhythm and high-gamma activity in macaque visual cortex. PLoS Biol. 9:e1000610.
Roberts MJ, Lowet E, Brunet NM, Ter Wal M, Tiesinga P, Fries P, De Weerd P. 2013. Robust gamma coherence between macaque V1 and V2 by dynamic frequency matching. Neuron. 78:523–536.
Roelfsema PR, Lamme VA, Spekreijse H. 2004. Synchrony and covariation of firing rates in the primary visual cortex during contour grouping. Nat Neurosci. 7:982–991.
Scheeringa R, Fries P, Petersson KM, Oostenveld R, Grothe I, Norris DG, Hagoort P, Bastiaansen MC. 2011. Neuronal dynamics underlying high- and low-frequency EEG oscillations contribute independently to the human BOLD signal. Neuron. 69:572–583.
Shadlen MN, Movshon JA. 1999. Synchrony unbound: a critical evaluation of the temporal binding hypothesis. Neuron. 24:67–77. 111–125.
Swettenham JB, Muthukumaraswamy SD, Singh KD. 2013. BOLD Responses in Human Primary Visual Cortex are Insensitive to Substantial Changes in Neural Activity. Front Hum Neurosci. 7:76.
Tallon-Baudry C, Bertrand O, Henaff MA, Isnard J, Fischer C. 2005. Attention modulates gamma-band oscillations differently in the human lateral occipital cortex and fusiform gyrus. Cereb Cortex. 15:654–662.
Thiele A, Stoner G. 2003. Neuronal synchrony does not correlate with motion coherence in cortical area MT. Nature. 421:366–370.
van Pelt S, Fries P. 2013. Visual stimulus eccentricity affects human gamma peak frequency. Neuroimage. 78:439–447.
Vidal JR, Chaumon M, O'Regan JK, Tallon-Baudry C. 2006. Visual grouping and the focusing of attention induce gamma-band oscillations at different frequencies in human magnetoencephalogram signals. J Cogn Neurosci. 18:1850–1862.
Wandell BA. 1995. Foundations of vision. Sunderland, MA: Sinauer Associates.
Wang XJ. 2010. Neurophysiological and computational principles of cortical rhythms in cognition. Physiol Rev. 90:1195–1268.
Welch P. 1967. The use of fast Fourier transform for the estimation of power spectra: A method based on time averaging over short, modified periodograms. IEEE Trans Audio Electroacoustics. 15: 70–73.
Whittington MA, Traub RD, Jefferys JG. 1995. Synchronized oscillations in interneuron networks driven by metabotropic glutamate receptor activation. Nature. 373:612–615.
Winawer J, Kay KN, Foster BL, Rauschecker AM, Parvizi J, Wandell BA. 2013. Asynchronous Broadband Signals Are the Principal Source of the BOLD Response in Human Visual Cortex. Curr Biol. 23: 1145–1153.
Womelsdorf T, Schoffelen JM, Oostenveld R, Singer W, Desimone R, Engel AK, Fries P. 2007. Modulation of neuronal interactions through neuronal synchronization. Science. 316:1609–1612.
Zhou Z, Bernard MR, Bonds AB. 2008. Deconstruction of spatial integrity in visual stimulus detected by modulation of synchronized activity in cat visual cortex. J Neurosci. 28:3759–3768.

Supplemental material

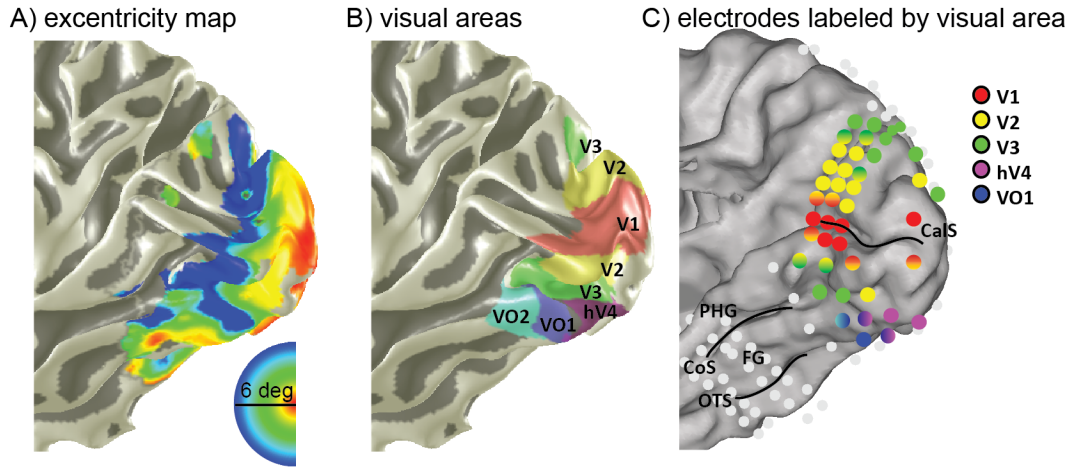

Figure S1: Visual areas in subject 1. **A)** Eccentricity map from fMRI scan (Winawer et al., 2013). **B)** Labels of visual areas derived from this visual field mapping experiment (eccentricity + polar angle maps). **C)** ECoG electrodes labeled according to the visual field maps, verified with ECoG. CalS = Calcarine sulcus, PHG = parahippocampal gyrus, CoS = collateral sulcus, FG = fusiform gyrus, OTS = occipital temporal sulcus.

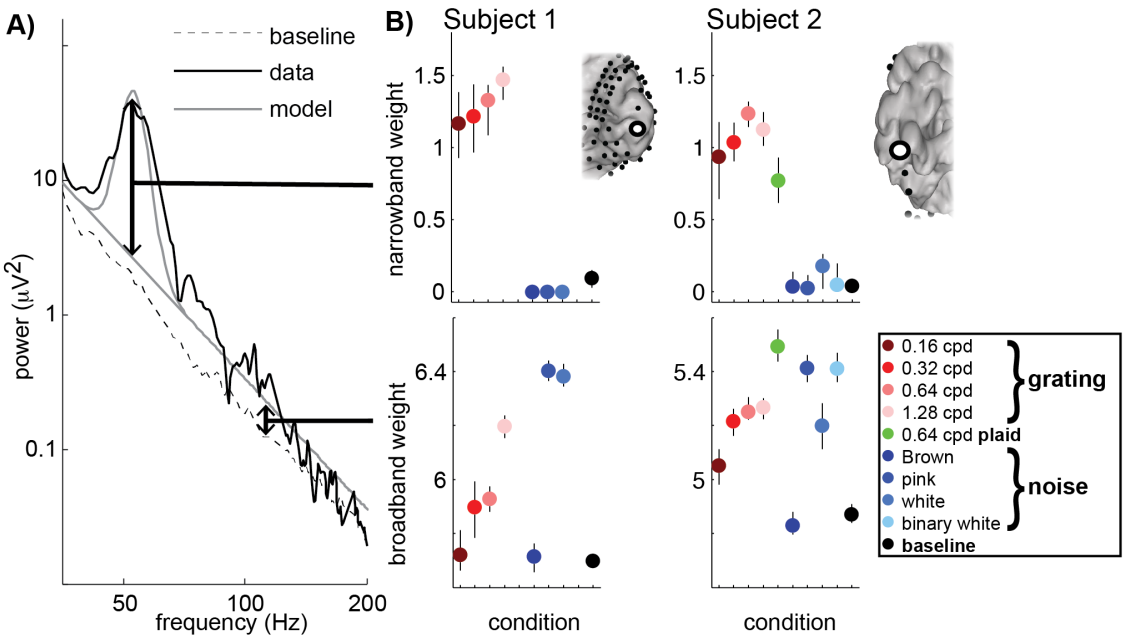

Figure S2: A) A power law plus Gaussian (model) was fitted to the average power spectra of each condition (data) in log-log space, resulting in respectively a weight for broadband plus narrowband increases compared to baseline. For each condition C with N_c trials, N_c trials were drawn randomly with replacement and averaged. The model (power law + Gaussian) was fitted to the average log power spectrum from these trials. This was repeated 100 times to calculate confidence intervals. **B)** For one early visual electrode in subject S1 and subject S2 the average narrowband and broadband weights and 95% confidence interval are shown.

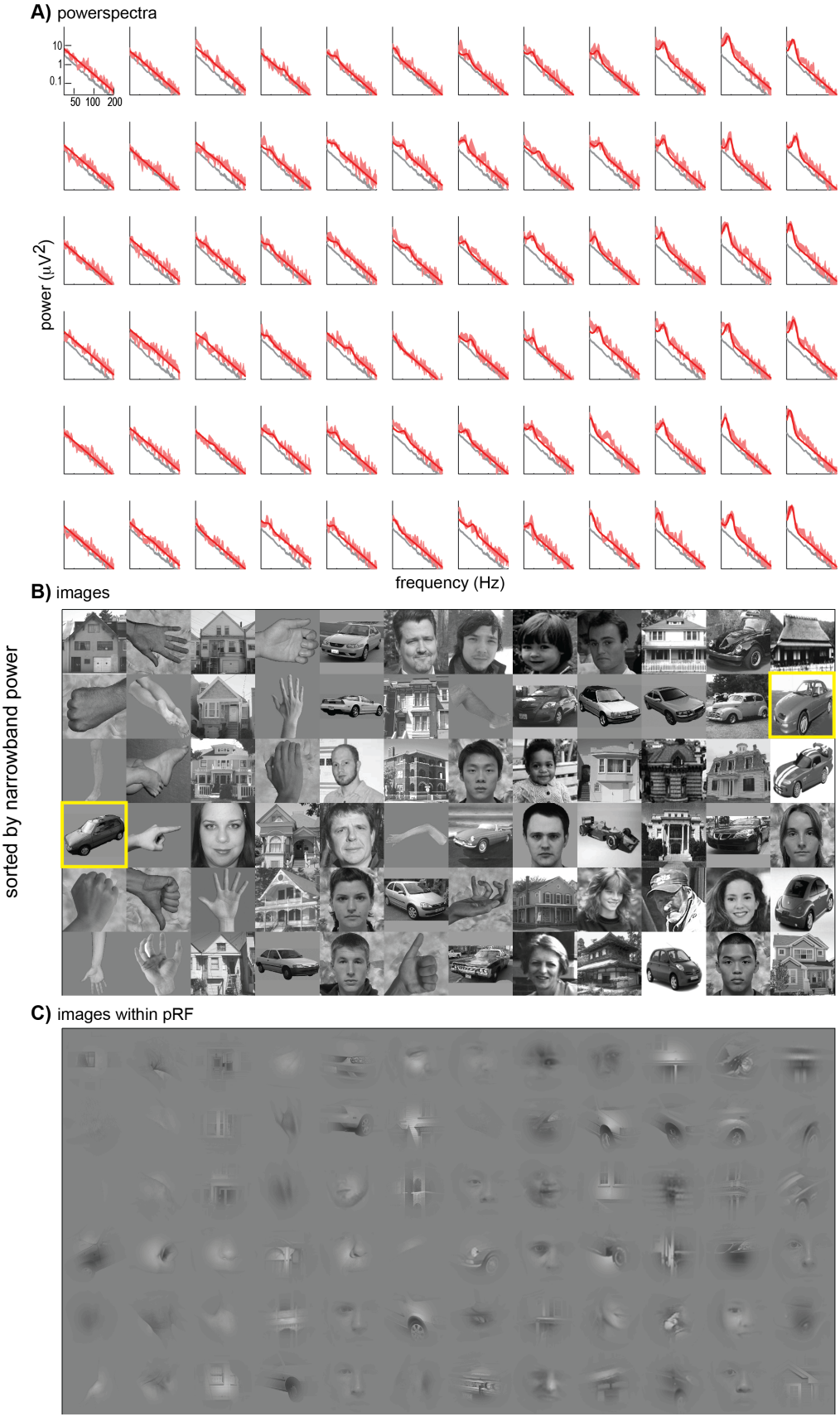
A) powerspectra
10
1
0.1
50 100 200
power (μV²)
frequency (Hz)
B) images
sorted by narrowband power
C) images within pRF

Figure S3: Power spectra and images ordered by narrowband power. Subject 3 viewed 72 images of faces, houses, cars and limbs, repeated 5-6 times each, while fixating a dot in the center of the screen (Parvizi et al., 2012, Jacques et al., 2013). All images (10x10°) were shown for 1000ms and the inter stimulus interval varied from 600-1400 ms. From an electrode in foveal V1 (determined by fMRI and ECoG retinotopic mapping, (Winawer et al., 2013)) the power spectra were calculated for the stimulus intervals and for a 500 ms pre-stimulus baseline. Power spectra were averaged across repeated images and were decomposed into narrowband gamma and broadband components (see Methods).

A) The 95% confidence intervals of the power spectra were calculated by bootstrapping the spectra of the repeated images 1000 times. These confidence intervals are displayed on a log-log plot ordered by narrowband gamma power with the smallest value in the upper-left, the largest value in the lower right, and decreasing down the columns and then rows. The confidence intervals are shown in light red and the baseline periods are shown in gray. The baseline is identical for every image. The model fits (power law plus Gaussian) are plotted as a red line. The images with yellow outlines are plotted in main text Figure 6. **B)** Images sorted by narrowband power, in same manner as A). **C)** Image windowed by the Gaussian population receptive field, sorted by narrowband power, as in A.

Broadband and narrowband estimates were reliable for the repeated images. If the model was fitted on the average power spectrum from the even and odd images the narrowband weights correlated with $r=0.78$ ($p<0.001$) and the broadband weights correlated with $r=0.79$ ($p<0.001$).

To estimate whether narrowband and broadband power was significant for each image, the power spectra for each image were bootstrapped 100 times and the model was fitted to estimate confidence intervals for the narrowband and broadband weights. If 95% confidence intervals were not overlapping with the confidence interval from the baseline period (gray), it was considered significant. Out of 72 images, 40 elicited significant gamma oscillations, 69 elicited significant broadband power increases. In the other foveal V1 electrode that was measured, 39 images elicited significant gamma oscillations, 68 elicited significant broadband power increases.

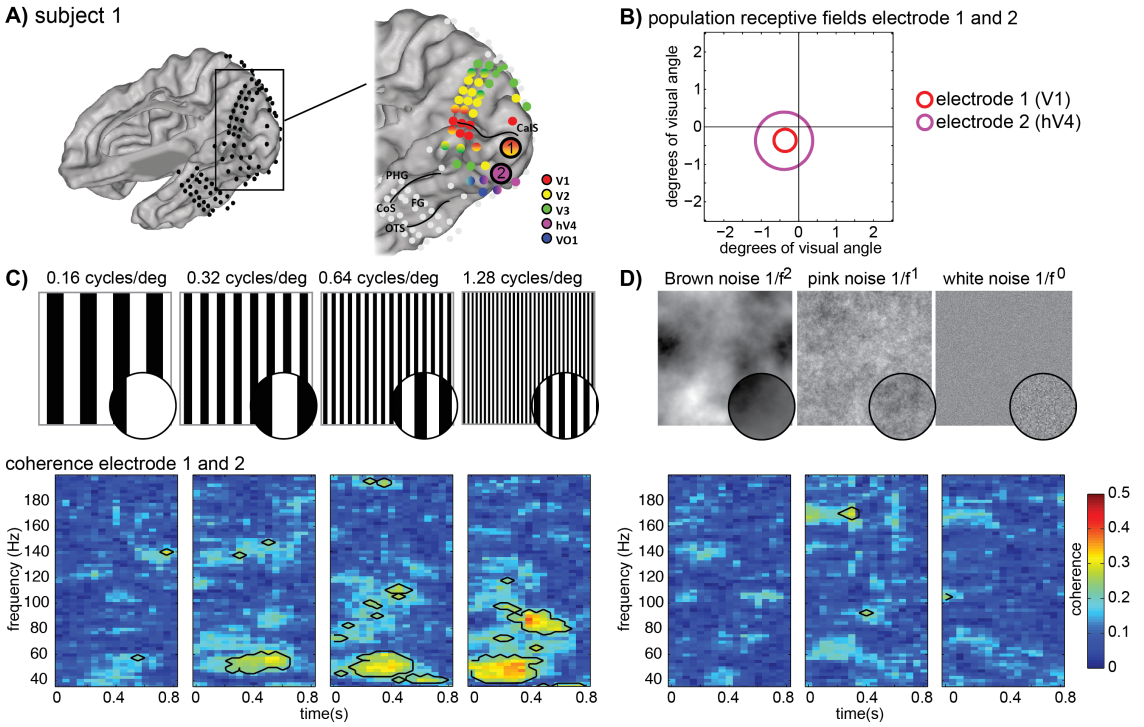

Figure S4: Coherence between V1 and hV4. Subject 1 had electrodes covering large areas of visual cortex and we calculated the coherence between two electrodes with overlapping population Receptive Fields (pRFs), one on the V1/V2 boundary and one on hV4.

To calculate coherence, we used the Chronux toolbox (http://www.chronux.org/, (Mitra and Bokil, 2008)). The coherence is the absolute value of the coherency *C(f)*: $C(f) = \frac{S_{XY}(f)}{\sqrt{S_{XX}(f)S_{YY}(f)}}$, where S_{xy} is the cross spectrum and S_{xx} and S_{yy} the power spectra for signals from 2 electrodes *X* and *Y*:

$S_{XY}(f) = \frac{1}{K}\sum_{k=1}^{K} X_k(f)Y_k^*(f)$, where Y_k* is the complex conjugate of Y_k.

$$S_{YY}(f) = \frac{1}{K}\sum_{k=1}^{K} |Y_k(f)|^2$$

$$S_{XX}(f) = \frac{1}{K}\sum_{k=1}^{K} |X_k(f)|^2$$

The power spectra and cross spectra of the signals x and y were calculated by the Fourier transform with 5 orthogonal Slepian tapers (Percival and Walden, 1993), for example for X_k:

$X_k(f) = \sum_{n=1}^{N} w_n(k)x_n e^{-2\pi i f t}$ where $w_n(k)$ is the k^{th} Slepian tapering function.

The coherence was estimated from 35 to 200 Hz in steps of 1 Hz, using a 400 ms window with 50 ms step size. The bandwidth of the tapers was set in such a way that there was a smoothing in the frequency range over +/-7.5 Hz.

A) Brain rendering with electrodes in subject 1. The electrodes on the V1/V2 boundary (electrode 1) and hV4 (electrode 2) are plotted larger. **B)** The pRFs from these two electrodes were derived from previous ECoG work (Winawer et al., 2013). The pRFs are plotted with 2 standard deviations around the center and are overlapping. Crosshairs are drawn on the center of the screen. **C)** Coherence between these two electrodes for gratings. **D)** Coherence between these two electrodes for noise patterns. The 95% confidence intervals were calculated by a Jackknife procedure and corrected for multiple comparisons across time and frequency. A black outline indicates that the 95% confidence interval did

not include zero. Note the clear presence of significant coherence in the gamma range (35-80 Hz) for the gratings.